CHAPTER 3

Human Presence Detection Behind the Wall*

*Part of This work has been published as:

Vineet Singh, Somak Bhattacharyya, and Pradip Kumar Jain, "Behind the Wall Heartbeat Detection using SVD and MTI Filtering." *2019 URSI Asia-Pacific Radio Science Conference (AP-RASC),* New Delhi, India, IEEE, pp. 1-4, 2019.

CHAPTER 3

Human Presence Detection Behind the Wall

In the previous *Chapter* 2, a simple technique exploiting the range and range resolution capability of an SFCW system to design a target localization system has been demonstrated. But, a sensing system with the ability to detect life signal enhances its capability and allows the user to make fast and correct decisions. This chapter aims to develop a processing algorithm that can determine the living human subject's life characteristics frequency. The capability of the system is further enhanced through-the-wall detection of live target presence in the range-Doppler plane.

In this chapter, an experimental study on through the wall human heartbeat detection using ultra-wideband continuous wave radar is carried out. In this regard, a stepped frequency continuous wave (SFCW) radar system is developed in the laboratory using a vector network analyzer (VNA) and a pair of horn antennas. The post-processing of the collected data is performed in two major stages. The first stage includes improving the received signal, which possesses the life sign information by improving the signal to clutter noise ratio. The later stage is dedicated to the detection of life characteristics in the range-Doppler (RD) plane.

3.1 Vital Life-sign Signature

Locating a human and detecting the vital signs such as breathing rate and heartbeat using a microwave sensor is a non-invasive technique. The human breathing rate lies in the range 0.2 to 0.5 Hz, while the range of the heartbeat rate is from 0.8 to 2.5 Hz. A composite model of heartbeat and breathing can be expressed as a bi-harmonic function, as shown in (3.1) [Zhou *et al.* (2009)].

$$r(\tau) = r_0 + A_H \sin(\omega_H \tau + \phi_H) + A_B \sin(\omega_B \tau + \phi_B) \quad (3.1)$$

where, $\tau > 0$, r_0 is the average distance and A_H , A_B are amplitudes, ω_H , ω_B are frequencies while ϕ_H and ϕ_B are initial phases of heartbeat and breathing, respectively. If the human subject is stationary, then three frequencies can be expected in the overall system viz., a zeroth-order frequency corresponding to stationary surrounding objects and two Doppler frequencies associated with heartbeat and respiration.

To achieve the desired objective using SFCW radar, it is necessary to understand the three basic concepts mentioned below. It is essential to know the coherent processing to apply the tactics of desired signal capture, and to understand the process to enhance the life sign signal enhancement and its vital sign retrieval from a radar return for a through the wall sensing condition where the clutter intensity is very much high in compared to the desired target associated response.

3.2 Coherent Processing

For a typical SFCW radar signal, the time-frequency plot is given in Figure 3.1. In SFCW radar, the signal sweeps all the (say *N*) frequency-points continuously entire operating bandwidth. While the time interval for each frequency tone is Δt , the sweep time T_S corresponds to $N \times \Delta t$. The time change in a single sweep is mainly dependent upon the systems analog to digital converter (ADC) and termed as fast sweep time. The total observation time to record all consecutive sweeps is known as the coherent processing interval T_{CPI} [Muñoz-Ferreras *et al.* (2017)]. A coherent processing interval (CPI) can be sampled with each sweep time T_S which is known as slow time. The transmitted signal $S_n(t)$ of *the* n^{th} frequency with round trip travel time *t* of a signal is expressed as [Amin (2017)]:

$$S_n(t) = Ae^{j2\pi(f_0 + n\Delta f)t} \quad (3.2)$$

However, $n\Delta t \le t \le (n+1)\Delta t \;;\quad n = 0,1,2,\ldots\ldots,N-1$ (3.3)

where the initial frequency is f_0, and A is the amplitude. Each signal dwells at each frequency step long enough to allow the reflected signal to reach the receiver. In such condition

$$\Delta t \ge \frac{2R_{\max}}{c} \quad . \tag{3.4}$$

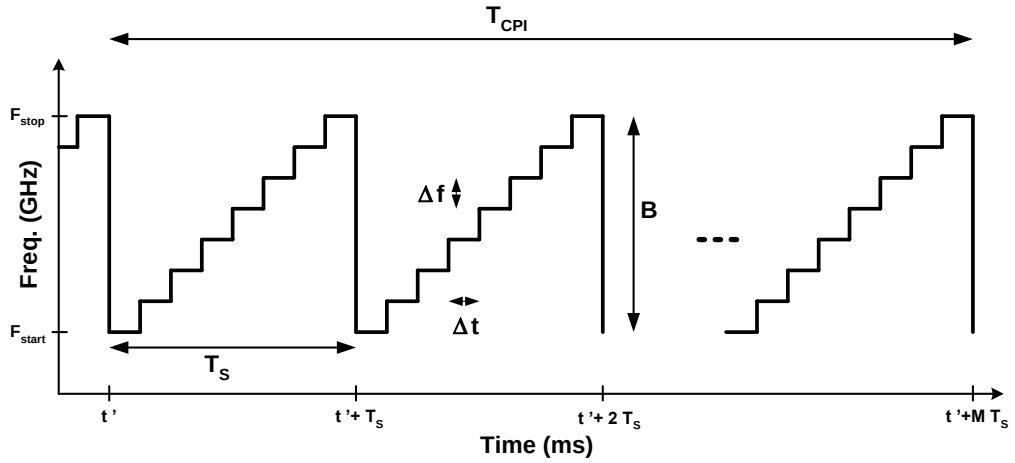

Figure 3.1: Time-frequency plot of the SFCW system for multiple consecutive sweeps.

3.2.1 System Implementation with a VNA

Since the used SFCW technique is implemented with the help of a vector network analyzer (VNA), it is necessary to understand the system level controlling parameters and constraints.

3.2.1.1 System Resolution Bandwidth (RBW)

An optimization algorithm runs inside the VNA to speed up the system by reducing sweep time efficiently. VNA does not allow to control the sweep time T_S directly. Thus in VNA, to control the sweep time, an alternative mechanism of controlling the size of the resolution bandwidth (RBW) and the number of frequency steps N in a single sweep are utilized. Fine RBWs and larger N increase the sweep time while increasing the

RBW and decreasing the N show the reverse effect and reduces the sweep time. In VNAs, RBW is one of the main parameters and controls, the resulting frequency spectrum resolution. The systems with smaller RBWs provide finer frequency resolution and have the ability to differentiate signals with closer frequency components. At the cost of system resolution bandwidth, the time-lapse to complete a sweep can be reduced. The number of frequency points *N* in a sweep further influences the sweep time T_s as the system becomes slower by increasing N's value.

3.2.1.2 Fast-time Sampling Frequency

The analog to digital converter (ADC) sampling rate is known as fast-time sampling frequency F_S. The target range is directly proportional to the baseband frequency F_b of the receivable down-converted echo signal. Hence to satisfy the Nyquist criterion and avoid aliasing, the system's sampling rate F_s must be greater than or equal to F_b. The following equation may calculate the frequency of the baseband signal F_b for a target at distance *R* as per the recommendation of Y.E Acar *et al*. (2020).

$$F_b = \frac{2BR}{cT_s} \quad , \tag{3.5}$$

where *B* is the sweep bandwidth and $T_s = 1/F_s$.

3.2.1.3 Operating Frequency and Bandwidth

In SFCW systems, small vibrational motions of the 'target' are perceived due to phase shifts in the returned signal. The phase change in a signal is directly proportional to its frequency. The wavelength becomes shorter at higher frequencies, resulting in a considerable variation in phase, even for a small change in frequency. In other words, by selecting a higher operating frequency, higher resolution can be achieved for target motion measurement. However, the use of smaller wavelength reduces the system

maximum range R_{max} as mentioned in equation (1.3), and such systems operating at higher operational frequency are not suitable for the applications demanding high range coverage or a medium with higher losses [(Acar *et al.* (2020)]. As per equation (2.5), SFCW systems with higher sweep bandwidth have increased range resolution, resulting in good spatial distance measurement accuracy.

3.3 Adopted Methodology

The adopted methodology can be seen as a combination of two stages, as shown in Figure 3.2. The first stage involves the data collection, while the second stage deals with the post-processing of the collected data.

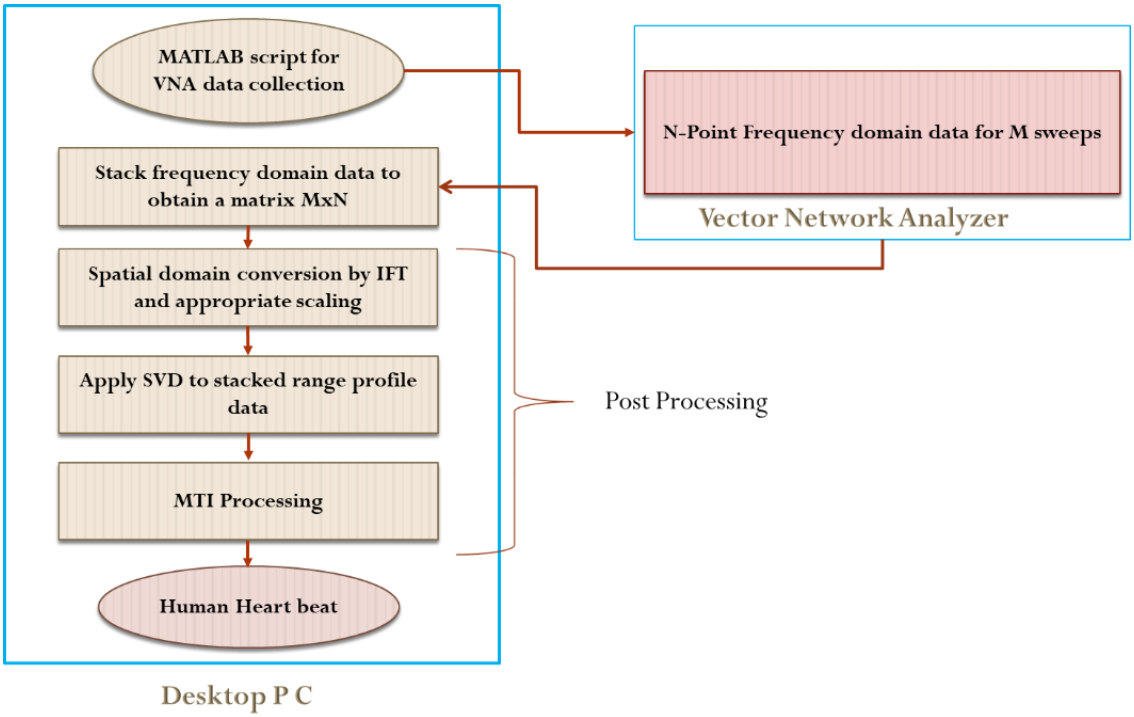

Figure 3.2: Command and data flow chart.

3.3.1 Data Capture

VNA is the core of the experimental setup, which contains all the processing related required modules within it. However, some functionalities that it cannot facilitate directly according to the user's needs are required to program. The modern network

analyzers are integrated with programming provisions. A user can interface the instrument with the PC using LAN wires, GPIB BUS, and USB cables using any interface environment. The Keysight N9916A is interfaced with PC using MATLAB instrument control toolbox for programming purposes in this work. Once the PC-VNA interface is established, the various data collection parameters have been transferred to the VNA memory using a MATLAB script file to perform the M-consecutive sweeps' data collection.

3.3.2 Post Processing

The collected frequency domain A-scan data has been converted to spatial domain range profiles and stacked to form a matrix of dimension $M \times N$ for vital sign processing, as shown in Figure 3.3. A singular value decomposition (SVD) based technique has been applied to mean difference images for relative enhancement of signals associated with human subject and suppressing the wall reflections. The human subject associated reflections is obtained in the second subspace of SVD also has the dimension of $M \times N$. Each column of the aforementioned retrieved data stored as $M \times N$ matrix form undergoes N- MTI filtering followed by Fourier transform successively, which yields the range-Doppler (RD) plane from where the life characteristics frequency can be easily obtained at a certain distance. The following subsections of Figure 3.3 give a better overview of the sequence of applied concepts in the post signal processing stage.

3.4 Clutter Reduction Techniques

The clutter reduction technique's role is essential to retrieving the target-related desired reflection and reducing the radar range profile's unwanted responses. Sometimes, through the wall/ hurdle life signature detection due to a high wall clutter, it becomes impossible to obtain the human subject reflected signals. The further signal processing

steps become useless to perform the characteristic frequency detections. In literature, the available techniques for removing clutter are singular value decomposition (SVD), principal component analysis (PCA), independent component analysis (ICA), factor analysis (FA), etc. Out of which SVD is applied, a statistics method of clutter removal method due to its simplicity for life characteristic containing signal enhancement.

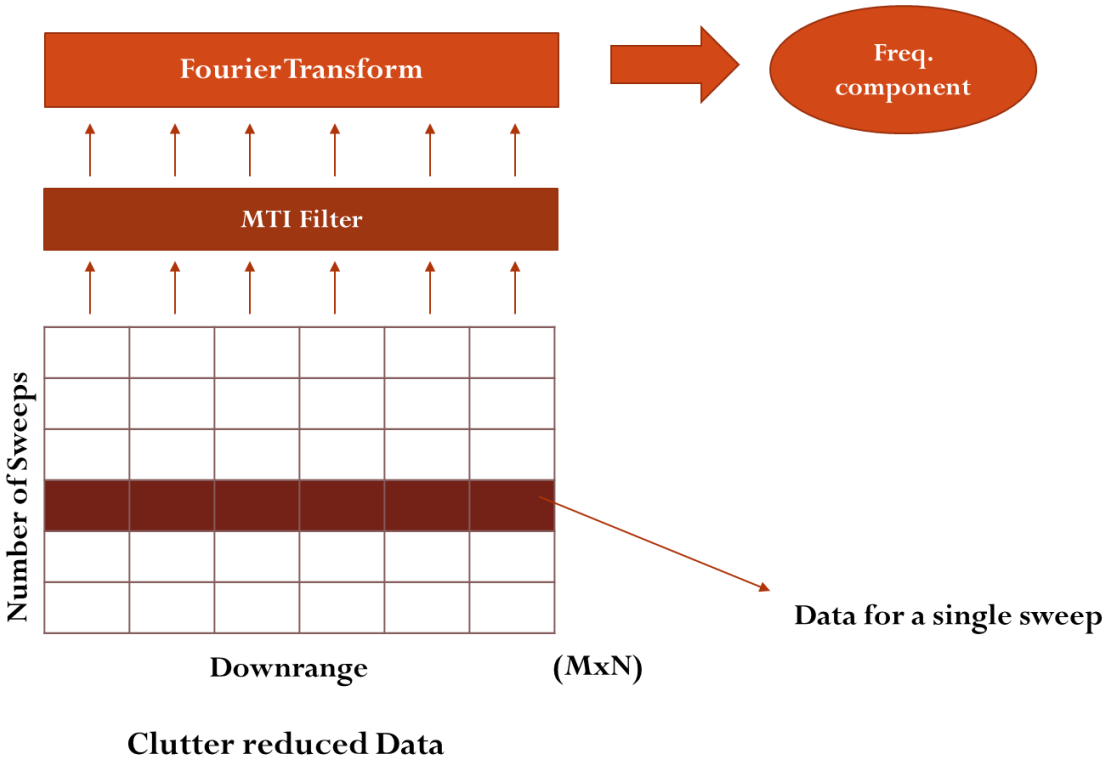

Figure 3.3: Data arrangement and vital sign frequency extraction process.

3.4.1 Singular Value Decomposition

SVD is widely used in the field of image processing and signal processing [Biglieri and Yao (1989), Sadek (2012)]. The purpose of the SVD based method is to enhance the signal to clutter ratio (SCR) by separating the data into the complementary subspaces called the target signal and clutter subspaces. It is the most effective and stable technique in linear algebra. Let a data stacked image is represented by $M \times N$ matrix (where $z = 1, 2.....M$ and $p = 1, 2.....N$). Here, z denotes the distance unit index in

downrange and *p* is the scan number. Since the distance index *z* is greater than the scan number *p*, therefore it can be assumed as *M* > *N*. Mean difference image *X* can be decomposed as:

$$\mathrm{X} = \mathrm{USV}^{\mathrm{T}} \tag{3.6}$$

Here, U and V are left-hand side and right-hand side unitary matrices with their size $M \times M$ and $N \times N$, respectively. The columns of U and V are known as the left-singular and right-singular vectors of *X*, respectively. The matrix S is a rectangular diagonal matrix of size $M \times N$ which contains singular values or weights (σ) of X as its diagonal elements satisfying the property of $(\sigma_1 \geq \sigma_2 \geq ..... \geq \sigma_{\mathrm{I}})$ with i^{th} diagonal entry where *i =1,2,..... I*. Since matrix U and V^{T} are unitary in nature, the columns of these matrices forms a set of orthonormal vectors, which can be considered as basis vectors. The mapping of the basis vector $\mathrm{V_i}$ to the stretched unit vectors $\sigma_{\mathrm{i}}\mathrm{U_i}$ is done by matrix X. According to the unitary matrix definition, the same holds true for their conjugate transposes U^{T} and V, except the geometric interpretation of the singular values as stretches is lost. The mean image matrix X can be decomposed in different subspaces as provided as:

$$\mathbf{X} = \mathbf{G}_1 + \mathbf{G}_2 + ... + \mathbf{G}_{\mathrm{N}} \quad . \tag{3.7}$$

The dimension of each decomposed sub-space is $M \times N$ which is similar to the original image matrix X. Some of these sub-spaces have target responses, and the rest contain non-desirable clutter information due to the wall and surrounding. Our aim is to identify the subspace containing the target response. In our case, we are getting a target response M_2 corresponding to σ_2, where the vector u_2 and v_2 are the second columns with a dimension of $M \times 1$ and $N \times 1$ of matrix U and V, respectively, as follows:

$$G_{target} = G_2 = \sigma_2 \times u_2 \times v_2^{T} \quad . \tag{3.8}$$

3.5 Moving Target Indicator (MTI)

The moving target indicator (MTI) based systems enhance the capabilities of basic radar systems to differentiate between the moving and static objects. To design such a system, it is desired to have the radar return nature in terms of frequency. The power spectrum of the static clutter can be represented by the delta function due to its zero Doppler frequency. However, clutter is not always constant. In practice, some Doppler frequency spread remains present due to small wind speed and other environmental and system movements. In general, the clutter spectrum is concentrated around dc frequency (f = 0), and integer multiples of the radar PRF f_r, and may show some small spreading. The power spectrum of a radar return in the clutter's presence and the target is shown in Figure 3.4 [Mahafza (2000)].

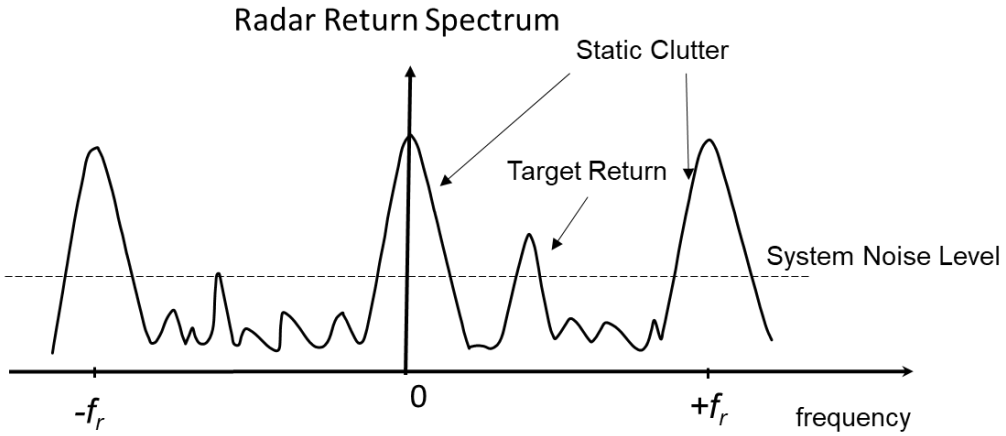

Figure 3.4: Radar return power spectral density (PSD).

In the case of CW systems, the static clutter is suppressed by omitting the receiver output around zero frequency, while in the case of a pulsed radar system, there is a requirement of a special type of filters to differentiate the targets with slowly moving, fast-moving, and stationery categories. Such types of filters are known as

moving target indicator (MTI). The aim of an MTI filter is to overcome target-like returns produced by clutter and allow moving target returns to passing through under minute or no degradation.

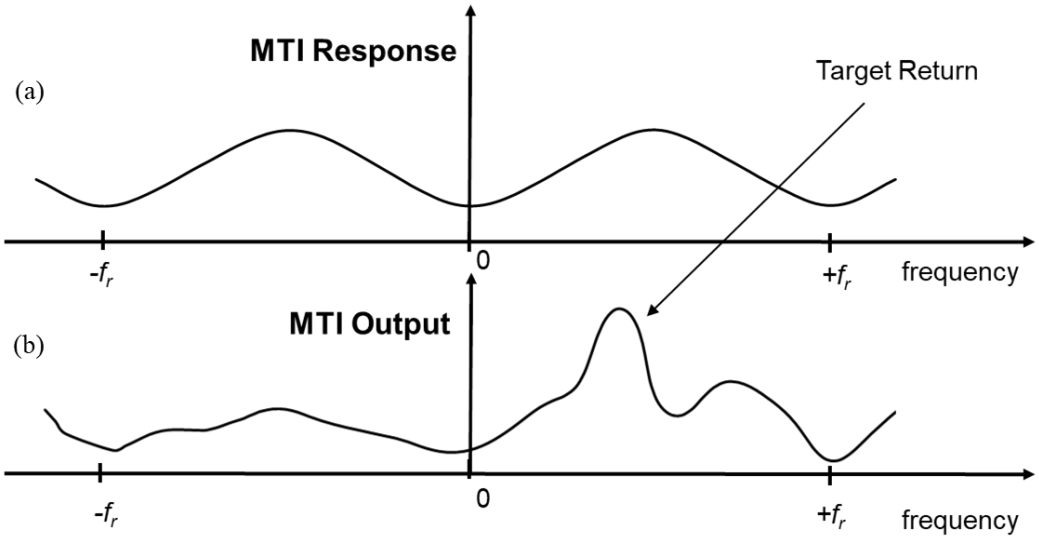

Figure 3.5: (a) Frequency response of an MTI filter; (b) Output from an MTI filter.

To deal with the clutter present in the radar return response, an MTI must have the frequency response, which contains a deep stop band around a DC (*f=0*) and multiple pulse repetition frequency f_r. A typical MTI and its output response are presented in Figure 3.5.

3.5.1 Types of MTI Filter

MTI filters can be implemented using delay line cancelers. The performance of different MTI schemes are compared to some predefined figure of merits like clutter attenuation (CA), MTI improvement factor (IF), and sub clutter visibility (SCV). MTIs are of mainly three types viz. (i) Single delay line canceler (ii) Double delay line canceler (iii) Recursive delay line cancelers.

Single delay line canceler is a basic MTI single delay-line, as shown in Figure 3.6(a). The time delay of a delay line is equal to the PRI.

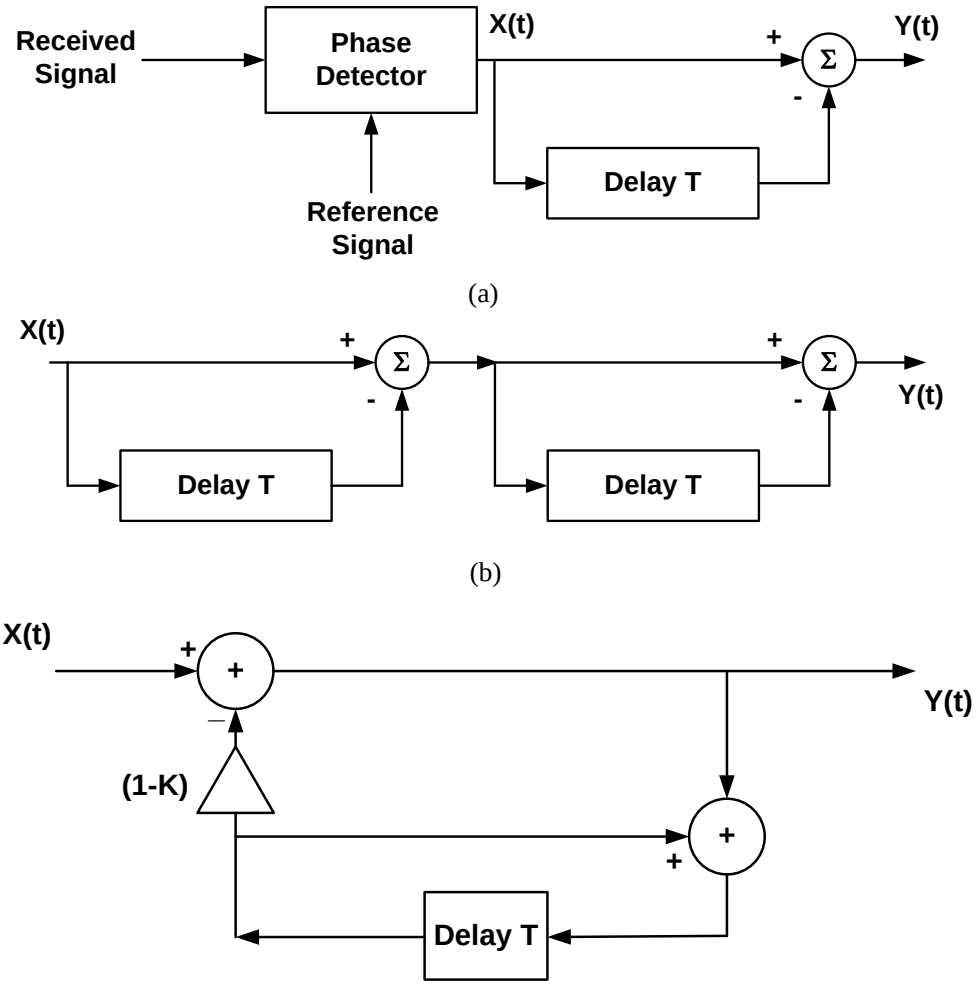

Figure 3.6: (a) Single delay line canceler; (b) Double delay line canceler and; **(c)** Delay line canceler with feedback.

The reference signal and the received signal are fed to a mixer that performs a phase detection function that provides the phase difference of the two input signals at the mixer-output [Li and Kiang (2004)]. The transfer function of a single delay line is:

$$H(z) = 1 - z^{-1} \quad . \tag{3.9}$$

Since single delay line cancelers do not have a wideband notch in the stopband, they are not acceptable in most radar applications. A double delay line canceler has a better response in both the stop- and pass-bands, and thus it is more frequently used than a single canceler. The basic unit configuration of a double delay line canceler is shown

in Figure 3.6 (b). Since it needs at least three pulses to produce the output, it is also termed as 'three pulse canceler' [Mahafza (2000)]. The transfer function of double line canceler is:

$$H(z) = (1 - z^{-1})^2 = 1 - 2z^{-1} + z^{-2} \quad . \tag{3.10}$$

A single delay line canceler with feedback is shown in Figure 3.6(c). It has the provision of feedback, which is also known as recursive filters. The feedback loop gain mainly governs the frequency response shape of the filter. The transfer function for the recursive MTI can be expressed in (3.10), where K is the gain factor, which controls the gain response. By increasing the value of K, the MTI filter response can be flattened. The filter with a flatter response has relatively more bandwidth, with the least gain variation in its pass-band:

$$H(z) = \frac{1 - z^{-1}}{1 - Kz^{-1}} \quad . \tag{3.11}$$

3.6 Experimental Setup

The ultra-wideband bi-static radar based on the stepped frequency continuous wave (SFCW) system is assembled with the help of VNA (Keysight-N9916A) along with a pair of identical horn antennas of C-band, RF coaxial cables, and connectors as illustrated in Figure 3.7. A human subject standing behind a plywood wall has been exposed in front of the bi-static radar system in rest conditions during the data collection. The wall's thickness was 1.1 cm, and its distance from the antennas was 2.0 m, and the distance and man to antenna distance were 2.5 m. The entire setup and the human subject are placed in an anechoic chamber so that the effects of other external environments could be minimized. MATLAB script is used to interface the VNA, and it was programmed to sweep from 4 GHz to 6 GHz following 201 linear frequency step

of other parameters of VNA and antenna systems are listed in Table 3.1. The frequency-domain data was collected for 400 sweeps for the antenna to subject distance of 2.5 m.

Table 3.1: Experiment specifications.

Sr. No.	Parameter	Value/specification
1.	Antenna Type	C-band Horn
2.	Source	Keysight FieldFox (N9916A)
3.	Freq. range	4-6 GHz.
4.	Range Resolution	7.5 cm.
5.	Transmitted power	-15 dBm
6.	Max. Unambiguous range	15 m.
7.	No. of points	201
8.	No. of sweeps	400

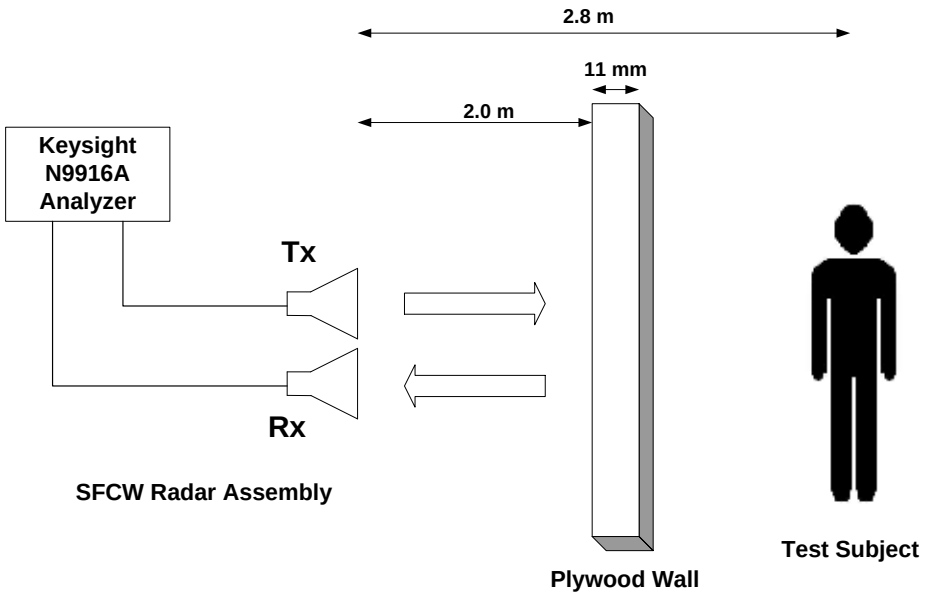

Figure 3.7: Experimental setup schematic placed within the anechoic chamber along with the human subject.

3.7 Results and Discussion

The electromagnetic wave radiated towards the human subject has to travel twice through the wall material, and it results in lowering the magnitude of subject-associated reflection.

For wall attenuation measurement, the insertion loss (IL) is calculated using (3.12) [Gaikwad et al (2011), Hussein, and Safaai-Jazi (2003)]:

$$IL = -20\log_{10}\left(S_{21wall} / S_{21air}\right) \quad . \tag{3.12}$$

Where S_{21wall} is S parameter measurement in presence of the wall and S_{21air} is S-parameter measurement in absence of the wall. For the plywood of 11 mm, the average attenuation value over a frequency band of 8-12 GHz wall was obtained as 1.1102 dB. Since the attenuation is very less and the maximum range measured value from the antenna was not much longer, any signal loss compensation was not used in the presented thesis work.

The ranging system used here is an SFCW system that acquire all the data in the frequency domain. The collected data has been translated to the spatial domain using expression (2.7), and the corresponding range profile has been obtained as given in Figure 3.8(a). Two major peaks have been observed in the single range profile, as shown in Figure 3.8(a), where the first peak appearing nearer to the antenna position is associated with wall reflection with a relatively higher amplitude while the other one corresponds to the human subject reflection and small in magnitude. In the range profile, all the measurements have been done in a downrange direction using the antenna as a reference. The wall and human subject peaks are obtained in the 29^{th} and 38^{th} range-bin, which correspond to the equivalent distance of 2.17 m and 2.85 m, respectively. The difference between these two distances (ranges) gives the distance of the wall and human subject.

All the 400 A-scans have been stacked together, as shown in Figure 3.8(b). Here, the range information is contained along *the y*-axis while the number of scans is represented on *the x*-axis, while the intensity in the image is represented by the color bar. The highest intensity in the stacked range-profile image appears with a yellow line, which is constant for all the scans and at a distance of 2.17 m, and it indicates the wall location.

However, line whose intensity is varying in the number of scan direction and at a constant distance of 2.85 m in downrange direction is representing the human subject position. The intensity variation occurs due to chest walls motion, which modulates the reflected wave phase and magnitude.

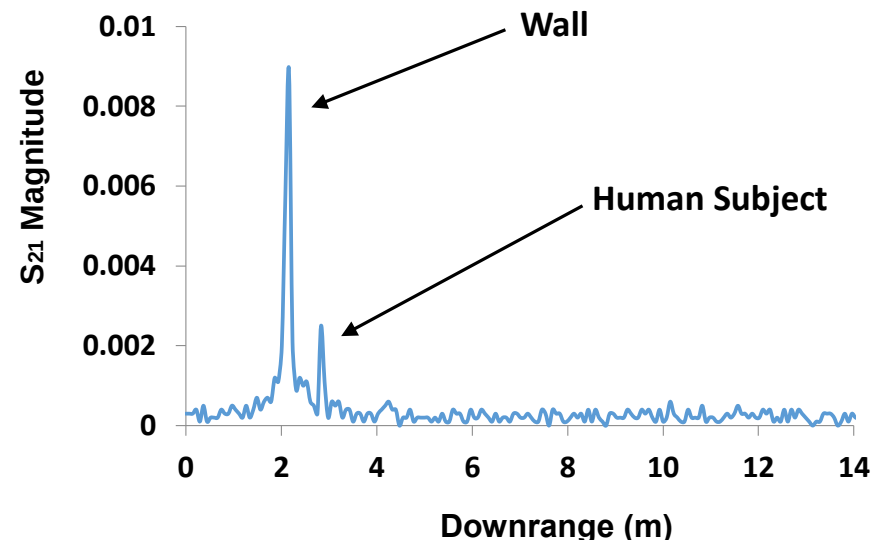

(a)

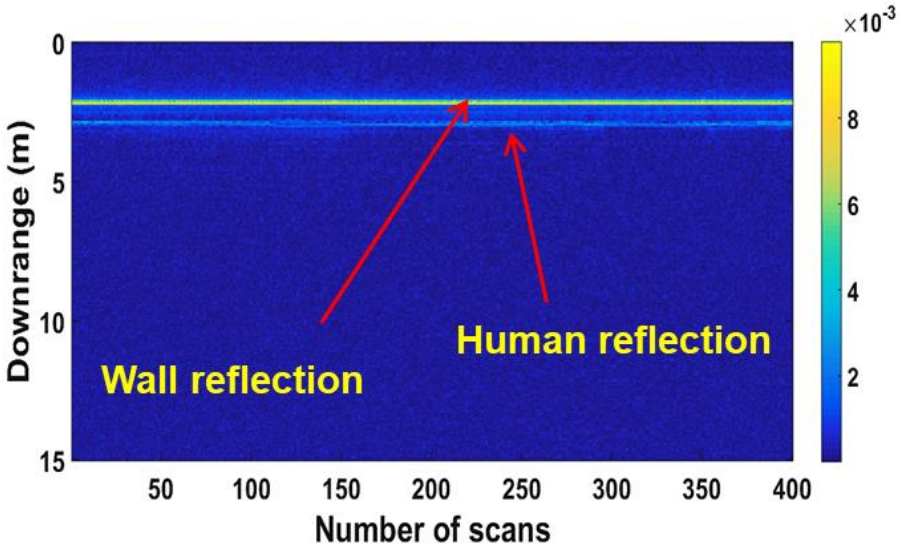

(b)

Figure 3.8: (a) Range profile generated from a randomly selected single sweep data; (b) Stacked data image by arranging the 400 range profiles.

The clutter reduced range profile using the SVD method eliminates the wall reflection completely from the range profile and enhances the human subject reflection significantly, as illustrated in Figure 3.9(a). The detailed effect on each A-scans is represented by Figure 3.9(b), where the wall reflections and background noise is absent while the subject associated reflections are preserved, which consists of life characteristics information. The signal to wall clutter ratio for the given scan in Figure 3.8(a) was 35%, and after SVD application, this improves to 489% for Figure 3.9(a).

To obtain the present frequency information in the clutter reduced data, the MTI processing has been applied, which eliminates the clutter coming from the static environment around the experimental setup as well as the static part of the human being in rest condition like head limbs etc. and allows only the signals reflected from moving parts. The value of clutter reduction associated with the static portion is 0.0194 dB. The Fourier analysis retrieves the present resultant RD plane is shown in Figure 3.10. It is observed from Figure 10 that life sign characteristics are present at 2.85 m away from the bi-static radar with a heartbeat frequency of 1.42 Hz.

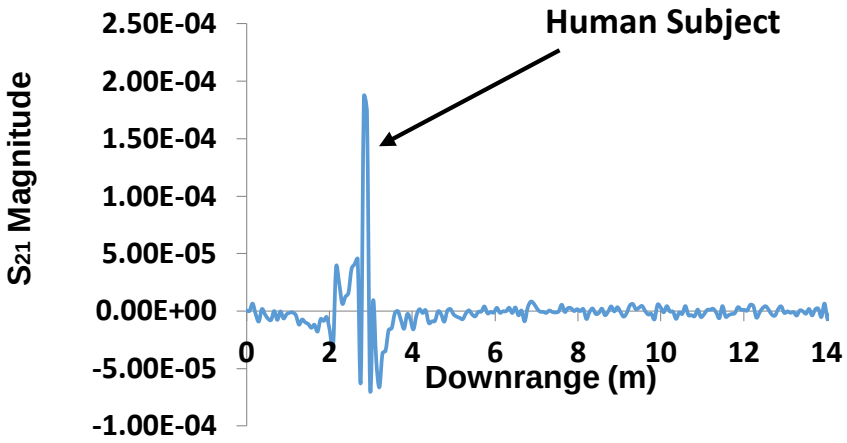

(a)

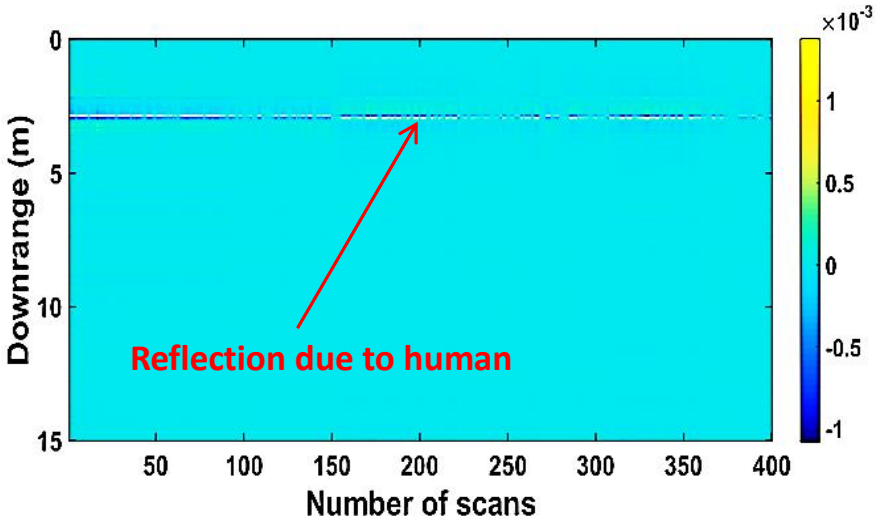

(a)

(b)

Figure 3.9: (a) Range profile generated from a single sweep data after clutter reduction; (b) Stacked data image by arranging the 400 range profiles after clutter reduction.

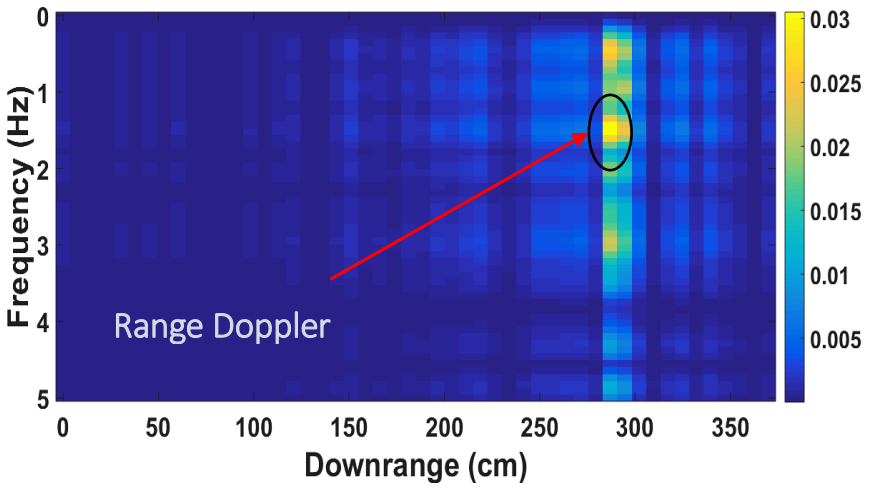

Figure 3.10: Detected human target location and heartbeat frequency in the range-Doppler (RD) plane.

3.8 Conclusions

The use of clutter reduction stage before to the moving target indicator (MTI) processing enables the vital sign monitoring system applicable for a practical purposes viz., military and victim search for disaster management purposes. The presence of a suspect or victim

in the down range from the radar is indicated. In present work, a C-band SFCW bi-static radar system has been synthesized in the laboratory operating over a frequency band of 4-6 GHz with the help of VNA and antenna. The developed radar was programmed to collect 400 consecutive sweep data in order to obtain the human heartbeat characteristic frequency. With the help of SVD based clutter reduction approach, the wall clutter in the multiple sweep stacked image was removed and hence the subject signal to wall clutter ratio, SCNR was improved from 35% to 489%. The MTI processing related to each common range bin was performed, and the human subject heartbeat rate 1.42 Hz at a distance of 2.85 m from the antenna was detected and represented in a range-Doppler (R-D) plane.